

The dependence of tidal stripping efficiency on the satellite and host galaxy morphology

Jiang Chang^{1,2*}, Andrea V. Macciò², Xi Kang¹

¹ *Purple Mountain Observatory, the Partner Group of MPI für Astronomie, 2 West Beijing Road, Nanjing 210008, China*

² *Max-Planck-Institut für Astronomie, Königstuhl 17, 69117 Heidelberg, Germany*

17 December 2012

ABSTRACT

In this paper we study the tidal stripping process for satellite galaxies orbiting around a massive host galaxy, and focus on its dependence on the morphology of both satellite and host galaxy. For this purpose, we use three different morphologies for the satellites: pure disc, pure bulge and a mixture bulge+disc. Two morphologies are used for the host galaxy: bulge+disc and pure bulge. We find that while the spheroidal stellar component experience a constant power-law like mass removal, the disc is exposed to an exponential mass loss when the tidal radius of the satellites is of the same order of the disc scale length. This dramatic mass loss is able to completely remove the stellar component on time scale of 100 Myears. As a consequence two satellites with the same stellar and dark matter masses, on the same orbit could either retain 60% of their stellar mass after 10 Gyrs or being completely destroyed, depending on their initial stellar morphology. We find that there are two characteristic time scales describing the beginning and the end of the disc removal, whose values are related to the size of the disc. This result can be easily incorporated in semi-analytical model. We find that the host morphology and the orbital parameters also have an effect on determining the mass removal, but they are of secondary importance with respect to satellite morphology. We conclude that satellite morphology has a very strong effect on the efficiency of stellar stripping and should be taken into account in modeling galaxy formation and evolution.

Key words: galaxies: evolution – galaxies: kinematics and dynamics – galaxies: interactions – methods: N-body simulations

1 INTRODUCTION

The current model for structure formation in the Universe is based on the cold dark matter (CDM) theory (White & Rees 1978; Blumenthal et al. 1984). In this hierarchical scenario small dark matter halos form first, and then they subsequently merge to form larger ones. At the same time, gas cools and collapses into the potential well of these dark matter haloes where star formation takes place, giving rise to the first protogalaxies. When dark matter haloes merge, these protogalaxies also merge; depending on the mass ratio the satellite galaxy can either rapidly merge with the central object or orbit around it for a consistent amount of time (e.g., Chandrasekhar 1943; Binney & Tremaine 2008; Jiang et al. 2008; Boylan-Kolchin et al. 2008).

In the second case the satellite galaxy will experi-

ence a progressive mass loss, both in its dark matter and stellar component (e.g., Mayer et al. 2001a; Klimontowski et al. 2007; Penarrubia et al. 2008; Kazantzidis et al. 2011). Observations have confirmed this scenario with the discovery of streams and complex stellar structures (shells and cusps) associated with the accretion and tidal disruption of satellite galaxies in our own Galaxy (e.g., Ibata et al. 1994; Yanny et al. 2000; Newberg et al. 2002; Majewski et al. 2003; Martin et al. 2004; Martinez-Delgado et al. 2005; Belokurov et al. 2006), in the Andromeda galaxy (Ibata et al. 2007; Ferguson et al. 2005; Kalirai et al. 2006), and beyond the Local Group (e.g., Malin & Hadley 1997; Forbes et al. 2003; Pohlen et al. 2004; Martinez-Delgado et al. 2012). In addition, the unbound stars from satellite galaxy are thought to be the origin of the diffuse intracluster light in clusters (Arnaboldi et al. 2002; Gerhard et al. 2005; Mihos et al. 2005; Gonzalez et al. 2000; Zibetti et al. 2005), and

* jchang@mpia.de

even in galactic stellar halo (Bullock & Johnston 2005; Bell et al. 2008; Carollo et al. 2010; Cooper et al. 2010).

These galaxy interactions can also lead to important morphological transformation in the satellite stellar distribution. Barnes (1992) showed that a stellar disc can be destroyed and form a hot, pressure supported spheroidal galaxy through tidal heating and violent relaxation during mergers. Moreover there is mounting evidence that environmental effects (e.g. tides and stripping) have an important role in shaping the properties of the local dwarf spheroidal galaxies (e.g., Einasto et al. 1974; Faber & Lin 1983; Mayer et al. 2001a, 2001b; Kravtsov et al. 2004; Mayer et al. 2006, 2007; Klimontowski et al. 2007; Penarrubia et al. 2008; Klimontowski et al. 2009a, 2009b).

The above two process, tidal stripping of satellite stars and morphology change in satellite remnant, have great impacts on the evolution of both satellite and central galaxy. For example, it is observationally found that massive central galaxies grow little in mass from $z = 1$ to $z = 0$ (e.g., Fontana et al. 2004), this seems to be in contrast with predictions based on the CDM model, where a large number of satellites should be accreted in this time interval. This observational result could be accounted for in galaxy formation models only if a considerable amount of the satellite stellar component is removed during the orbit, before the merger actually happens. (e.g., Monaco et al. 2006; Somerville et al. 2008; Kang et al. 2008). Moreover knowing the mass (stellar and dark matter) of the satellite before the merger is crucial to correctly model the effects of the merger itself, like remnant morphology, induced star formation etc. (e.g., Kauffmann et al. 1999; Cole et al. 2000). Thus a full understanding of the evolution of satellite galaxy, in term of their mass removal and morphology change, is important to correctly model galaxy formation.

A number of studies have used numerical N-body simulations to investigate the influence of environments on satellite evolution, both on cluster mass scales (e.g., Moore et al. 1999; Gnedin 2003; Mastropietro et al. 2005), and on Milky Way-like mass scales (e.g., Mayer et al. 2001a,b; Klimontowski et al. 2009a; Kazantzidis et al. 2011). Recently Vilalobos et al. (2012) have presented a very thorough study, covering a broad parameter space, on the effects of environment on the satellite galaxies in group environment.

In this paper we use N-body simulations to study the effect of the initial satellite and central galaxy morphology on the efficiency of tidal stripping and mass loss. We adopt three different morphologies for the satellite: pure disc, pure bulge and the combined one with 80% of stellar mass in the disc. We also employ two morphologies for the central galaxy, namely pure disc and the combined bulge+disc. We vary the orbit of the satellite, changing the angle of the orbital plane with respect to the central disc, and we test both prograde and retrograde orbits. The paper is organized as follows. §2 describes the numerical methods and the parameters we used. §3 shows the results for different satellite morphologies, different host morphologies, and different orbit parameters. Conclusions and discussion are presented in §4.

2 NUMERICAL METHODS

The parameter space describing galaxy mergers is very wide, since it includes several structural parameters defining the merging galaxies as well as the orbital parameters of the merger itself. In this work we have decided to concentrate our attention on the effects of morphology on stellar and dark matter mass removal. We will then keep the mass (stellar and dark matter) of the host and the satellite fixed through this paper, while we will vary how the stellar mass is distributed within both galaxies. The initial conditions are created using the same approach as in Springel et al. (2005), the simulations are evolved with the GADGET2 code (Springel et al. 2005) and we use SUBFIND to identify the bound structures. Here below more details on all those three steps are provided.

2.1 Initial Conditions

Each galaxy is composed of a dark matter halo and a stellar component. The dark matter halo is modeled with a Hernquist density profile (Hernquist 1990):

$$\rho_{\text{dm}}(r) = \frac{M_{\text{dm}}}{2\pi} \frac{a}{r(r+a)^3}, \quad (1)$$

where a is the radial scale length. We require the this density profile to be the same of a NFW one (Navarro, Frenk and White 1997) with the same total mass. Under this requirement there is a one to one correlation between the a parameter and the scale radius (r_s) of the NFW profile:

$$a = r_s \sqrt{2[\ln(1+c) - c/(1+c)]}, \quad (2)$$

where c is the concentration parameter, defined as $c = r_{200}/r_s$, and r_{200} is the radius at which the mean enclosed dark matter density is 200 times the critical density.

We tight the halo concentration to the halo mass using the well known concentration-halo mass relation, with the parameters given in Macciò et al. (2008). We fix the mass of the primary halo to be $10^{12} M_{\odot}$ and the mass of the satellite to $10^{11} M_{\odot}$. The spin of the dark matter halo is fixed to be $\lambda = 0.03$ for both halo masses, in good agreement with results from cosmological simulations (e.g. Macciò et al. 2007).

The stellar mass of each galaxy is set using the halo-stellar mass relation from Moster et al. (2010), based on the abundance matching techniques. For the masses considered in this work, this implies that the primary galaxy has a stellar mass of about 3% of its total halo mass, and satellite has 1% of halo mass in stars. Table 1 contains a detailed list of all parameters we kept fixed in all our runs.

For the distribution of the stellar component in each galaxy we employ three different morphologies:

- A rotationally supported disc galaxy (D). The stellar disc has an exponential surface density profile with scale-length h , and Spitzer's isothermal sheet with scaleheight z_0 . The three-dimensional (3D) stellar density in the disc is hence given by

$$\rho_{\star}(r, z) = \frac{M_{\star}}{4\pi z_0 h^2} \text{sech}^2\left(\frac{z}{2z_0}\right) \exp\left(-\frac{R}{h}\right) \quad (3)$$

- A non-rotating spheroidal bulge galaxy (B). The stellar bulge has a Hernquist density profile (see eq. 1).

Table 1. Properties of the primary and satellite galaxies

	“Primary”	“Satellite”	
DM Halo			
Virial mass (M_{200})	0.96×10^{12}	1.1×10^{11}	(M_\odot)
Virial radius (r_{200})	160	80	(kpc)
Concentration (c)	6.8	8.3	
spin parameter (λ)	0.03	0.03	
Number of particles	8×10^5	8×10^5	
Softening (ϵ_h)	0.3	0.1	(kpc)
Stellar (disc & bulge)			
Mass (M_*) ⁽¹⁾	3%	1%	
Number of particles	6×10^5	2×10^5	
Softening (ϵ_s)	0.07	0.02	(kpc)

(1): M_* for the stellar mass in unit of the virial mass of dark matter halo (M_{200}).

- A composed galaxy with both Hernquist bulge and an exponential disc (C). The bulge contains 20% of the total stellar mass unless stated otherwise.

From now on, we will use the capital letter “C”, “B” and “D” to describe the morphology of the primary (host) galaxy, and use “c”, “b” and “d” for the satellite. For example, an C-d merger will indicate a the merger between a composed primary galaxy (disc+bulge) and a pure disc satellite galaxy. More details can be found from Table 2.

The disc scalelength h is set by relating it to the angular momentum J_d of the disc, assuming strict centrifugal support of the disc and negligible disc thickness compared with its scalelength, so we have:

$$J_d = M_d \int_0^\infty V_c(R) \left(\frac{R}{h} \right) \exp \left(-\frac{R}{h} \right) dR \quad (4)$$

where $J_d = (M_*/M_{DM})J$ by assuming that the disc has the same specific angular momentum as the dark matter halo. The disc scaleheight z_0 is set as $z_0 = 0.2h$. A complete list of all parameters describing the stellar component can be found in Table 2.

2.2 Orbital parameters

For each experiment, the satellite galaxy is initially released at the virial radius of the primary galaxy with velocity (V_r, V_ϕ), where $V_r = v_r V_{200}$ and $V_\phi = v_\phi V_{200}$ are the radial and tangential components of the initial velocity, respectively. V_{200} is the circular velocity at the virial radius of the central primary galaxy. Our reference orbit has been set with $(v_r, v_\phi) = (0.9, 0.6)$ as suggested by results based on cosmological simulations (Benson 2005). We also explore more “circular” or “radial” orbits by changing v_r and v_ϕ .

If disc galaxies are used for the central and/or the satellite, there are further degrees for freedom that are related to the angles between the two discs and between the satellite disc and the orbital plane. These three angles are described in Figure 1.

A detailed list of all the orbital parameter used in the different merging simulations can be found in Table 3.

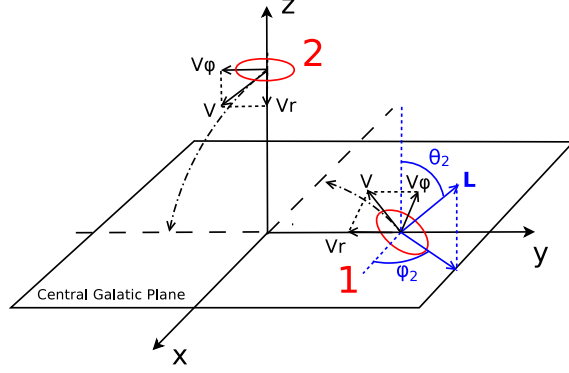


Figure 1. Initial satellite galaxy position and velocity in the primary galaxy frame. V_r and V_ϕ are the radial and tangential components of the initial velocity, respectively. Case 1 represents a coplanar orbit with respect to the primary galaxy disc, with the satellite polar angle $\theta_r = 90^\circ$. \mathbf{L} indicates the angular momentum of stellar disc. θ_2 & φ_2 are the azimuthal and polar angle of \mathbf{L} . Case 2 represents orbit perpendicular with $\theta_r = 0^\circ$.

Table 3. Orbit parameters.

Label	Host	sat.	(v_r, v_ϕ)	θ_2	φ_2	θ_r
C-c	C	c	(0.9,0.6)	0	0	90°
C-cR ⁽¹⁾	C	c	(0.9,0.6)	180	0	90°
C-cB	C	cB	(0.9,0.6)	0	0	90°
C-cD	C	cD	(0.9,0.6)	0	0	90°
C-cT	C	cT	(0.9,0.6)	0	0	90°
C-cc ⁽²⁾	C	c	(0.6,1.1)	0	0	90°
C-cr ⁽³⁾	C	c	(1.2,0.3)	0	0	90°
C-d	C	d	(0.9,0.6)	0	0	90°
C-dT	C	dT	(0.9,0.6)	0	0	90°
C-dR	C	d	(0.9,0.6)	180	0	90°
C-dTR	C	dT	(0.9,0.6)	180	0	90°
C-b	C	b	(0.9,0.6)	0	0	90°
C-bL	C	bL	(0.9,0.6)	0	0	90°
C-b45	C	b	(0.9,0.6)	0	0	45°
C-b90	C	b	(0.9,0.6)	0	0	0°
B-c	B	c	(0.9,0.6)	0	0	90°
B-d	B	d	(0.9,0.6)	0	0	90°
B-b	B	b	(0.9,0.6)	0	0	90°
C-dv0 ⁽⁴⁾	C	d	(0.9,0.6)	90	0	90°
C-dv90	C	d	(0.9,0.6)	90	90	90°
C-dv180	C	d	(0.9,0.6)	90	180	90°
C-dv270	C	d	(0.9,0.6)	90	270	90°

(1): “R” for Retrograde encounter, the same below. (2): “r” for more “circular” encounter with orbital eccentricity $e = 0.6$. (3): “c” for more “radial” encounter with $e = 0.97$. (4): “v” for “vertical” disc with the polar angle of angular momentum of the disc $\theta_2 = 90^\circ$ respected to the orbit plane.

2.3 Bound and unbound mass of the satellite galaxy

Here we describe our procedure to find the bound mass of the satellite galaxy along its orbit. At each time step we: (i) pick up all the stellar particles of the satellite by their IDs, and get the position with the highest density. (ii) Get the

Table 2. Stellar morphologies

	“Primary”				“Satellite”						
Morphology	BULGE	COMPOSED	bulge		composed				disc		
	B	C	b	bL ⁽⁸⁾	cB ⁽⁹⁾	c	cT ⁽¹⁰⁾	cD ⁽¹¹⁾	d	dT ⁽¹²⁾	
$M_{disc}^{(1)}$	0	0.8	0	0	0.7	0.8	0.8	0.9	1.0	1.0	(M_\star)
$j_d^{(2)}$	0	0.024	0	0	0.007	0.008	0.005	0.009	0.01	0.006	
$R_s^{(3)}$	0	3.01	0	0	1.59	1.59	1.04	1.59	1.60	1.01	(kpc)
$N_{disc}^{(4)}$	0	4.8	0	0	1.4	1.6	1.6	1.8	2.0	2.0	(10^5)
$M_{bulge}^{(5)}$	1.0	0.2	1.0	1.0	0.3	0.2	0.2	0.1	0	0	(M_\star)
$a^{(6)}$	0.61	0.62	0.29	0.72	0.32	0.32	0.32	0.21	0	0	(kpc)
$N_{bulge}^{(7)}$	6.0	1.2	2.0	2.0	0.6	0.4	0.4	0.2	0	0	(10^5)

(1): M_{disc} for the stellar disc mass in unit of total stellar mass M_* . (2): j_d for the disc spin parameter. (3): R_s for disc scale length. (4): N_{disc} for the particles number of disc. (5): M_{bulge} for the stellar bulge mass in unit of total stellar mass M_* . (6): a for bulge scale length. (7): N_{bulge} for the particles number of bulge. (8):“L” for Larger with $a = 0.72kpc$. (9):“B” for more Bulge with mass fraction $M_{bulge} = 0.3M_{star}$. (10):“T” for Thicker disc than reference disc (see R_s). (11):“D” for more Disk with disc fraction $M_{disc} = 0.9M_{star}$.

mean velocity of all particles within the radii R_{core} (“core”) around the density peak, and it is taken as the background velocity. (iii) Compute the gravitation potential energy E and kinetic energy K of each particles, for both star and dark matter, in the core’s frame, and if $E < K$, the particle is unbound, and removed from the remnant. (iv) Repeat the previous step until the remnant has converged. We assume that if the remnant has stellar particles less than 25, the satellite is totally disrupted. Those unbound particles are stripped by the tidal force from the host galaxy.

The only free parameter in the above procedure is R_{cor} used to define the “core” size. In our simulation we adopt $R_{core} = 0.1Kpc$, and we found that our results are stable to the slightly changing of R_{core} by a few factor. A too large or small R_{core} will result in large fluctuation on the remnant mass during the satellite evolution.

3 RESULTS

3.1 Effects of satellite morphology

The time evolution of satellite stellar mass density is shown in Fig. 2. The upper panels are for a satellite with pure disc (d), while the lower ones for satellite with pure bulge (b). The primary galaxy is always at the center of each panel (labeled with a cross) and its stellar component is not shown.

The upper panels show that, at beginning of galaxy approach (left panel, $t=1$ Gyr), the satellite still remains its initial disc shape (the disc is face-on in this projection). A prominent tidal feature appears soon after the second pericentric passage ($t=5$ Gyrs). Such tidal features are very common during the galaxy interactions (e.g., Toomre & Toomre 1972; Dubinski et al. 1996). Much more twisted tidal tails can be seen after a few pericentric passages (the upper right, $t=8.0$ Gyrs). The galaxies then is completely disrupted at $t=8.5$ Gyrs.

The situation is different in the lower series of panels where the evolution of a pure bulge satellite is shown. After the second pericentric passage ($t=5.0$ Gyrs) the tidal features are very weak, they become then more evident at $t=8.0$ Gyrs (third panel), but even in this case the satellite

still retains more than 80% of its initial stellar mass. Finally the satellite is able to survive to tidal force for the whole simulation time (10 Gyrs) with a total stellar mass loss of less than 40%.

By simply looking at Figure 2 it is already evident that satellite morphology plays a key role in shaping stellar stripping.

We quantify these different behaviors in Fig.3, where the evolution of the stellar mass (solid lines), halo mass (dotted lines) and distance from the center (dashed lines) is shown for the three different satellite morphologies (keeping fixed the morphology of the central galaxy, C).

The comparison of the solid with the dotted lines show that the stripping of the dark matter halo is quite different from that of the stars. At the first pericentric passage, the halo has lost its mass by around 50%, while stars are practically untouched. The removal of the stellar component starts only after having lost 80-90% of the dark matter mass. The stellar mass loss is always slower than the dark matter one, and the satellites becomes more and more stellar mass dominated with time (we will come back on this issue later). The above results are very similar to the recent ones obtained by Villalobos et al. (2012). These authors run a series of simulation of satellite orbiting in a “group” environment. They also find that the satellite DM halo lose mass quickly than the disc, and after the first pericentric passage, the halo has lost around 50% of its initial mass.

Let’s now look at the stellar mass loss. At the initial stage of the merger the stellar mass is somehow shielded by the dark matter halo and no stripping is present for ≈ 5 Gyrs. After the third pericentric passage the stellar mass loss begins. The C-d and the C-c merger show a similar mass loss for 1.5 Gyrs, while the b satellite is able to retain a larger fraction of its stellar mass. Things change dramatically at $t \approx 7.2$ Gyrs, when the mass of the satellite in the C-d scenario drops by more than two orders of magnitude in less than 200 Myrs, with the satellite being practically destroyed at $t \approx 8$ Gyrs.

The C-b run has a complete different behavior, with the satellite able to retain more than 60% of its mass at the end of the simulation run ($t = 10$ Gyrs). The C-c case is

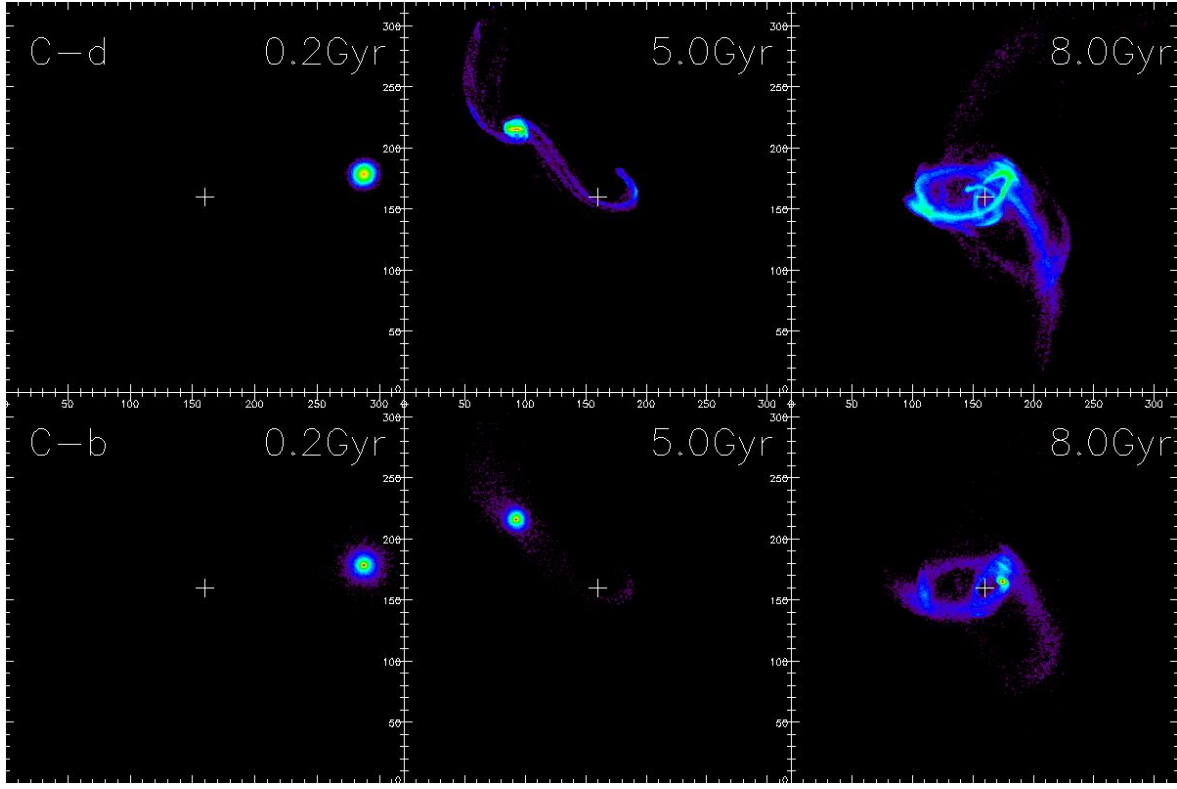


Figure 2. Time evolution of the stellar component of satellite galaxy. The cross indicates the center of the primary galaxy. The upper panels shows the C-d merger, while the lower one is the C-b merger. The unit of the coordinate is kpc, and the color shows the density.

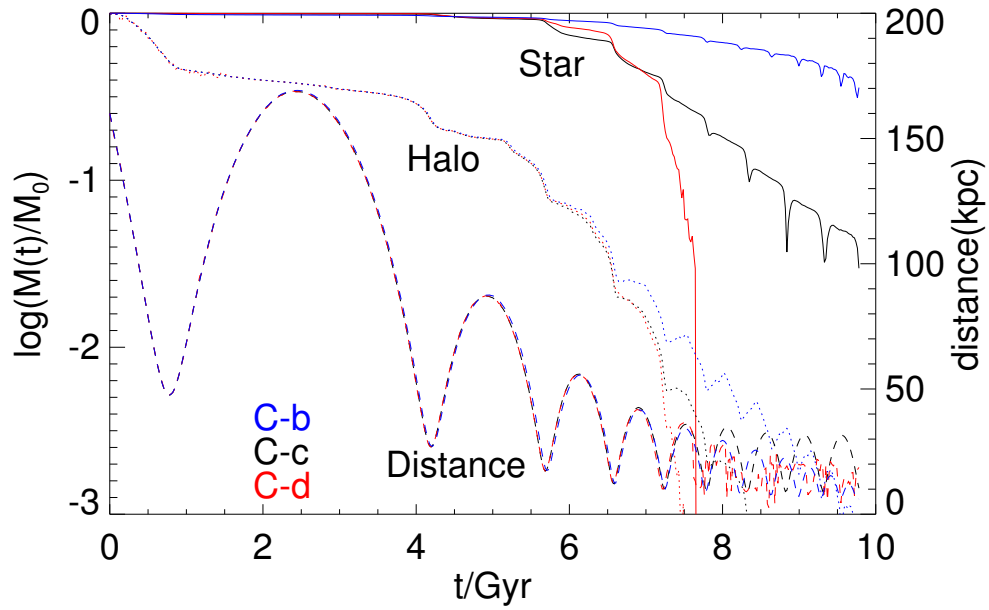


Figure 3. The distance and remnant bound mass fraction as a function of time for 3 different satellite morphologies merging with a bulge + disc host. The solid lines show the evolution of stellar mass, while the dotted shows one of the dark matter component. The dashed lines indicate the distances between satellite and center host galaxy.

somehow in the middle; it experiences a strong mass loss in the initial phase (when the disc is removed), but then is able to retain up to 20% of its initial bulge mass till $t = 10$ Gyrs. Our results are in fair good agreement with Villalobos et al. (2012). One difference is for the composed (bulge + disc) case where Villalobos et al. found a faster stripping with respect to a pure disc case. The reason for this discrepancy lies in the fact that Villalobos et al. “added” the bulge to the disc hence changing the total stellar mass. While in our cast M_* is a constant. A larger mass implies a different orbital evolution and then a different mass loss rate. From Fig.3 it is clear that the satellite morphology has a very strong impact on its tidal disruption. Two satellites with the same stellar and dark matter mass, on the same orbit could either retain 60% of their mass after 10 Gyrs or being completely destroyed only depending on the initial stellar morphology.

3.2 Tidal radius and disc scale length

We want now to look deeper in time evolution of the disc mass in the C-d merger. Our goal is to understand what sets the specific moment in time when the disc experiences the exponential stellar mass loss shown in Fig.3. As a first thing we compute the tidal radius for satellites. We define the tidal radius (R_t) according to Binney & Tremaine (2008) as the distance between the Lagrange point, L_3 , and the center of the satellite. We then define the tidal mass (M_t) as the mass the mass within R_t . With this definition we find a good agreement between the tidal mass and the bound mass (see section 2.3), as shown by the dashed and the solid lines in the four panel of Fig. 4. The slightly offset between the two curves is due to non-instantaneous removal of the mass outside R_t , as previously found by in other studies (e.g., Taylor & Babul 2001; Zentner & Bullock 2003; Gan et al. 2010).

We found two characteristic time scales: the first one determines the beginning of the tripping effect and it is set by the time when the tidal radius is equal to 10 times the disc scale length (t_{10R_s}), the second one marks the moment when the stellar tidal stripping becomes exponential, this happens when the tidal radius is of the same order of the disc scale length (t_{R_s}). These two time scales are marked by vertical arrows in the upper left panel of Fig. 4.

In order to test whether these time scales are really independent from the actual value of R_s we run second simulation with a thicker disc (C-dT) with a smaller scale length. Results are shown in the right upper panel of Fig. 4, where we find that t_{10R_s} and t_{R_s} are still able to capture the transition between different stripping regimes (this also applies for runs with different orbital parameters see Fig. 8.)

According to our results there are two time scales for disc galaxies the first one (τ_{life}) defines the life time of satellite stellar disc, the second one (τ_{strip}) defines the time from the beginning of the stellar tidal stripping to the complete disruption of the satellite, in formulas:

$$\tau_{life} = t_{R_s} - t_{acc} \quad \tau_{strip} = t_{R_s} - t_{10R_s}. \quad (5)$$

Where t_{acc} is the time of accretion of the satellite onto the main halo. Note that our definition of τ_{life} is different from the conventional ones, such as the total satellite dynamical friction time-scale. This time scale should be incorporated

in models of galaxy formation, to predict the stellar mass loss for the disc of satellite galaxy.

On the other hand we do not find a specific time scale for the bulge disruption (as shown in lower panels of Fig. 4 for two simulations with different bulge scale lengths). The bulge mass removal seems to have a constant efficiency that we expect to be orbital dependent.

3.3 Satellite mass profile and morphological evolution

As the satellite loses its mass due to tidal stripping, its inner structure and morphology also change. In Fig.5 we show the evolution of dark matter density profile of the satellite in the C-d, C-c and C-b cases. During the first 2.5 Gyrs (one pericentric passage) the dark matter density profile only changes in the external part ($R \gtrsim 10$ kpc) with no effects on the inner part. When the number of pericentric passages increases the density profile start to change also in the inner region ($R \approx 2$ kpc) with a constant dropping of the central density value. After 6 Gyrs the evolution of the dark matter density profile is linked to the evolution of the stellar component: for composed and bulge satellite, the contribution to the overall potential due to the stellar component is able to retain more dark matter in the center. On the contrary for the disc satellites the very quick removal of the stellar component also affects the dark matter distribution, that drops by two orders of magnitude in its central density at $t = 7.4$ Gyrs. This in qualitative agreement with previous results by Kazantzidis et al. (2004, 2011), even if a direct comparison is difficult given the larger mass ratio they assumed for their (1:100 and 1:1000) satellites and the different orbital parameters.

Fig. 6 shows the evolution of the stellar surface density of the satellite. The inner surface density of satellites “c” and “b” is practically unchanged during the whole evolution. The outer part of satellite “c” decreases significantly, as a consequence of the removal of the disc component, and at the end the composed satellite galaxy transforms in a pure bulge galaxy. For satellite “d” (left panel), the inner profile actually increases by about 20% during the first few pericentric passages, but then decreases dramatically at the latest stage of the evolution (7.4 Gyr), with a central density reduced by more than one order of magnitude. The initial increase in the central density in the disc case is due to the formation of a bar-like structure after the first passage.

A more clear understanding of the morphological evolution can be seen in Fig. 7. For the disc case it is evident the formation of a central concentration (bar-like) after the first passage (4.9 Gyrs), and the subsequent quick dissolution of the stellar component. For the composed galaxy the evolution from disc dominated to bulge dominated is also quite evident, with the disc being completely removed after 6.8 Gyrs. Finally the bulge case does not show any appreciable change on the inner stellar distribution, but just a progressively mass loss in the external part.

3.4 Dark Matter/Stellar mass evolution

Figure 3 clearly shows that the dark matter mass is removed more efficiently than the stellar component, is than worth to

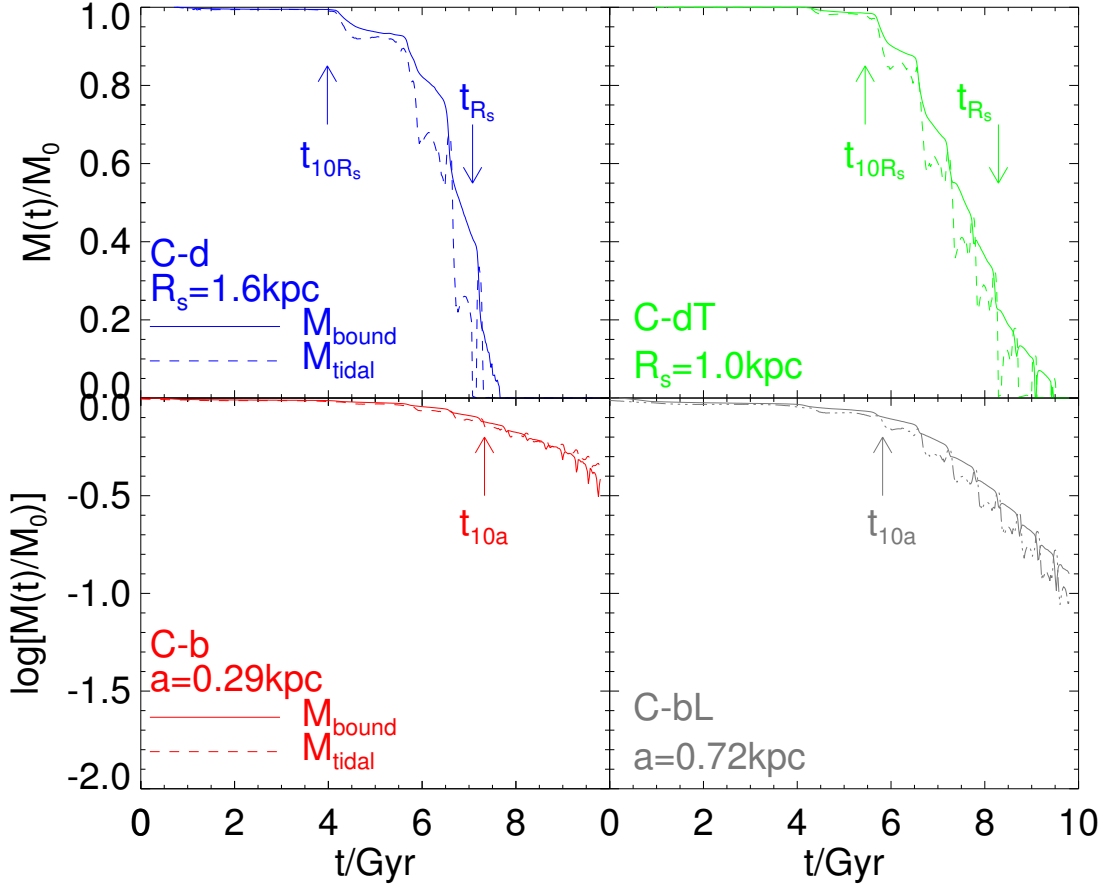


Figure 4. The correlation between tidal mass and bound mass. The left upper panel shows the evolution of remnant bound mass M_{bound} (solid line) and the mass within tidal radius M_{tidal} (dashed line) of a disc satellite. The upward arrow shows the time t_{10R_s} when $R_{tidal}(t_{10R_s}) = 10R_s$, and the downward arrow shows t_{R_s} when $R_{tidal}(t_{R_s}) = R_s$. The upper right panel shows the same thing but for a thick disc satellite with $R_s = 1.0 \text{ kpc}$. Bottom panels show the evolution for bulged satellite for different values of a (left $a = 0.29$, right $a = 0.72$).

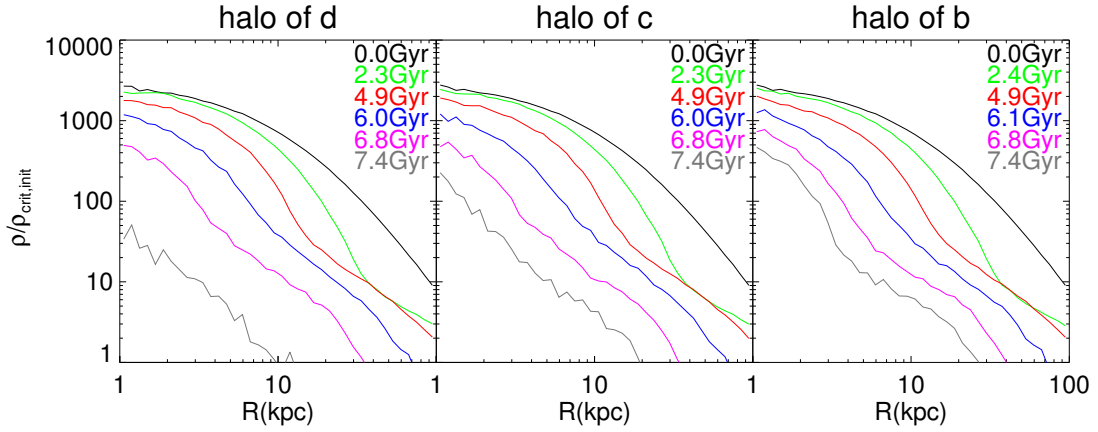


Figure 5. The evolution of the dark matter density profile for three different satellite morphologies. From left to right are “d”, “c” and “b”. The density profiles are shown at different apocentric passages.

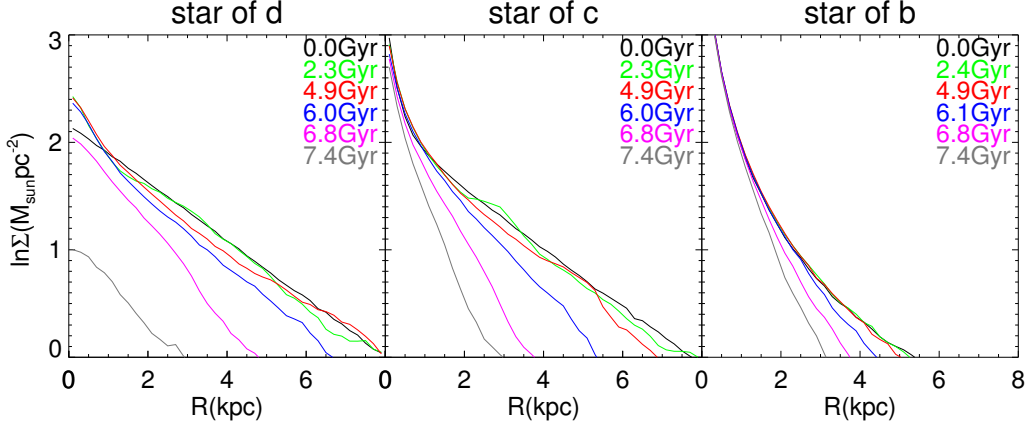


Figure 6. The evolution of the surface density profile of stellar component for three different satellite morphologies. From left to right are “d”, “c” and “b”. Also the density profiles are shown at different apocentric passages.

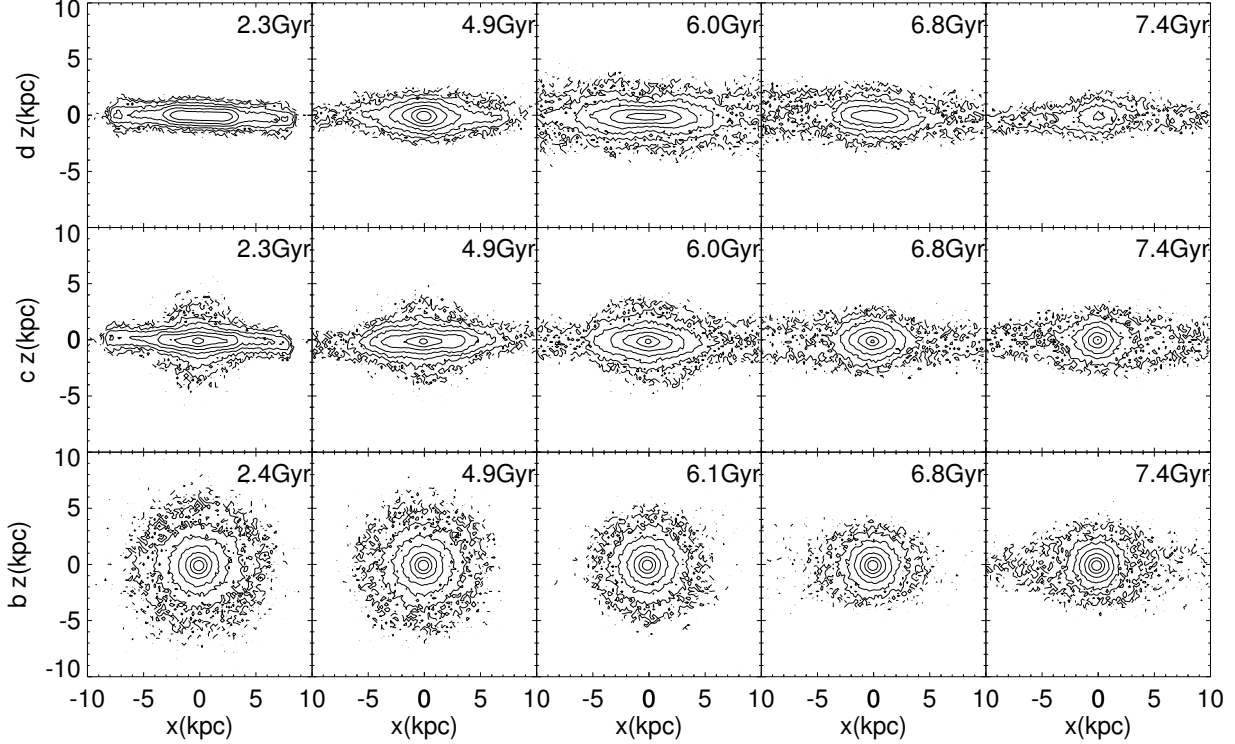


Figure 7. Evolution of isodensity contours for the satellite “d”, “c” and “b” (from top to bottom). The contours are plotted at the same levels.

look at the time evolution of the ratio between dark matter and stellar mass in our simulations. Recently a new form of stripping (dubbed *resonant stripping*, D’Onghia et al. 2009) has been proposed. In this formalism the disc angular momentum can couple with the orbit angular momentum, as a consequence the stellar particles within the disc can be stripped by the tidal force more effectively than dark matter, possibly creating a dark matter dominated satellite. Since we expect this angular momentum coupling to happen only for prograde encounters, we run an additional retrograde C-d simulation.

The evolution of the mass removal and of the dark to stellar ratio is shown in Figure 8. We do not find any evi-

dence for resonant stripping, even if we do find that prograde mergers are marginally more effective in inducing tidal stripping effects as well known in the literature (Cox et al. , 2006). We also find that the dark-to-stellar ratio has a monotonic behavior and that the satellite becomes more and more stellar dominated as time goes by, due to the removal of the external dark matter envelop. It is also worth noticing that our time scales (t_{10R_s} and t_{R_s}) are still able to determine the mass loss evolution.

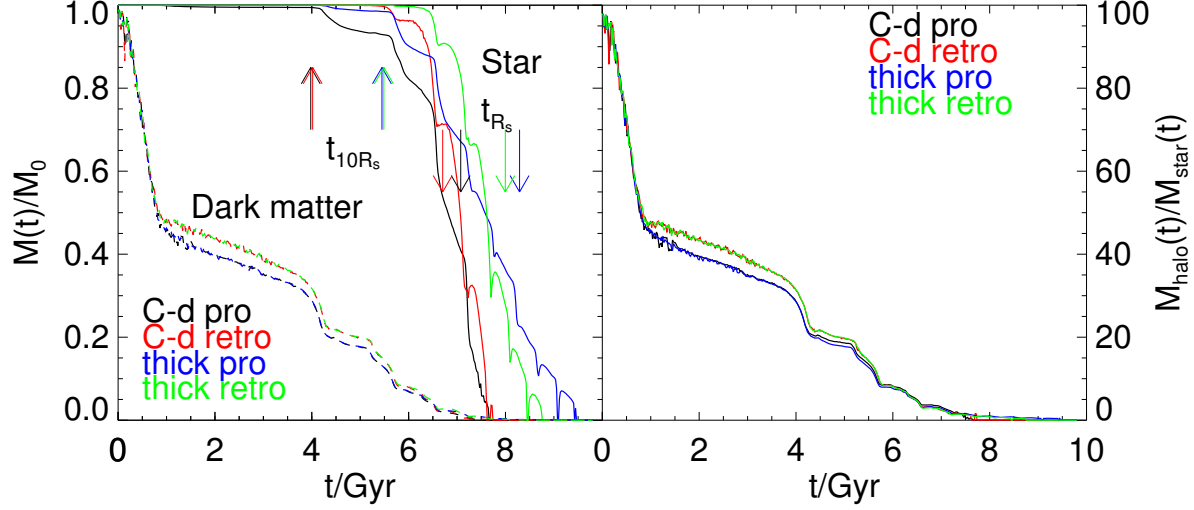


Figure 8. The left panel shows the evolution of bind mass of prograde and retrograde of two kind of different morphologies. The dashed line is the dark matter and solid line is the stellar, and the upward arrows show the time of t_{10R_s} of different mergers. The right panel shows the mass ratio between dark matter and stellar mass.

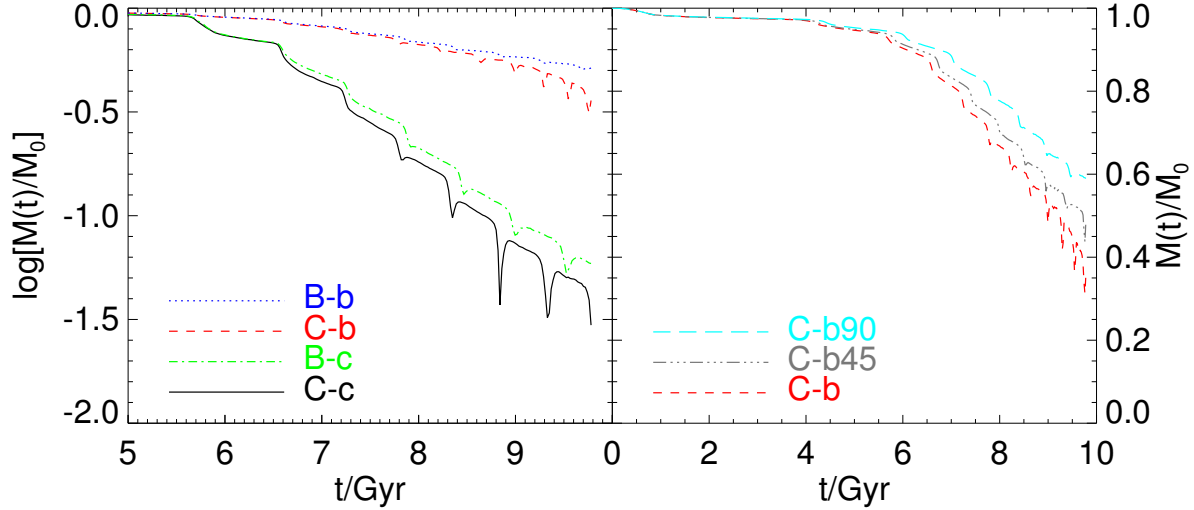


Figure 9. The left panel shows the effect of the host morphology on the mass loss of a “b” satellite(upper lines) and “c” satellite(bottom lines). The morphology of host galaxy has a second order of effect on the remnant mass of satellites compared to the morphology of satellites themselves. The right panel shows the evolution of the stellar mass for different orbit polar angles θ_r (see Table.3).

3.5 Dependence on host morphology and satellite orbit

In previous sections, we have investigated the dependence of tidal stripping on satellite morphology. In this part we examine the effects of central host galaxy morphology and the orbit of satellites. The effect of the host galaxy model on stellar stripping is shown in the left panel of Fig. 9. For a fixed satellite morphology (compose of bulge) the effect of the central galaxy is very mild, with the a composed (bulge+disc) morphology being more effective in inducing tidal stripping (see for example the difference between the blue and the red curve or between the green and black one). This effect is due to the more extended stellar component in the “C” case and to its the more asymmetric potential.

If the central galaxy has a stellar disc, the orbit of the

satellite may have different inclination, θ_r , with respect to this central disc. In the right panel of Fig. 9 we plot the evolution of the stellar mass loss for a satellite in an orbit coplanar with the disc ($\theta_r = 0^\circ$, red), perpendicular to disc ($\theta_r = 90^\circ$, cyan), and in between with $\theta_r = 45^\circ$ (grey).

As expected the tidal stripping is the strongest (weakest) for the coplanar (perpendicular) orbit. On the other hand this effect is quite small and the angle between the orbital plane and the galactic disc seems to not play a major role in determining the tidal stripping.

Finally we test a few cases for satellites on more radial or more circular orbits. Our results are consistent with previous studies (Boylan-Kolchin et al. , 2008) that a more radial (eccentric) merger leads to a faster mass loss. On the other hand we do not find any particular trend between the orbit

and the satellite morphology; this implies that our previous results also apply in the case of different orbits.

4 DISCUSSION AND CONCLUSIONS

In this work, we used N-body simulation to study how the morphology of satellite and central galaxy effect the tidal stripping in a series of isolate minor mergers.

We kept all parameters of the merger (stellar mass, dark halo mass and orbital parameters) fixed while we experiment with three different morphologies for the satellite: pure disc, pure bulge and bulge+disc and two for the host galaxy: bulge+disc and pure bulge.

In agreement with previous studies we find that the removal of the stellar component only begins after the satellite dark matter halo has lost a consistent fraction of its mass, of the order of 90%.

We find that for a fixed stellar mass, the morphology of the satellite has a very strong effect in determining its final stellar mass after several orbital periods. Depending on its initial stellar distribution a satellite can either survive to the tidal forces from the central halo retaining a consistent fraction of its mass, or being completely disrupted.

We find that there are two characteristic time scales that define the stellar stripping of a pure disc satellite. The first one sets the beginning of the stellar stripping (after the removal of the outer dark matter envelope) and happens when the tidal radius is of the order to ten times the scale radius of the disc. The second one sets starting of the very quick removal of the disc component (exponential mass loss) and occurs when the tidal radius is of the order of the disc scale length. These two time scales are quite insensitive to the actual value of the disc scale lengths and to the merger orbital parameters. They can then be very useful to define the stellar stripping of disc like satellites in models aiming to describe galaxy formation.

For a composed morphology (disc+bulge) we find that the disc component is quickly removed as in the pure disc case and then the remaining bulge is able to survive for a longer time.

The morphology of the central galaxy has only a second order effect on the tidal stripping, with a bulge+disc model being slightly more effective in removing dark and stellar mass from the satellite.

Finally we look at effects of the angle between the orbital plane and the central galactic disc. As expected satellite moving in the plane of the disc experience a somehow stronger mass loss than satellite moving perpendicular to the disc. But again we find that the effect of the orbit orientation is sub-dominant with respect to the satellite morphology.

The effect of satellite morphology on the tidal stripping, usually neglected in the galaxy formation models, could have important effects on the predictions of the diffuse stellar light in galaxy groups and clusters, as well as the abundance of disc dominated satellites. Our results imply that only satellites with a substantial bulge can survive for a long time, while disc dominated satellites, is still present, should have been accreted recently. We plan to address in details the effects of stellar stripping on galaxy formation and evolution in a forthcoming paper.

ACKNOWLEDGMENTS

We kindly thank Volker Springel for providing the code to set up the initial galaxy for our simulation run. The numerical simulations used in this work were performed on the THEO cluster of the Max-Planck-Institut für Astronomie at the Rechenzentrum in Garching. The authors acknowledge support from the MPG-CAS through the partnership program between the MPA group lead by A. Macciò and the PMO group lead by X. Kang. AVM acknowledges funding from the Deutsche Forschungsgemeinschaft via the SFB 881 program "The Milky Way System". Xi Kang is supported by the NSFC (No. 11073055), National basic research program of China (2013CB834900), the foundation for the author of CAS excellent doctoral dissertation, and the Bairen program of CAS. J. Chang acknowledges support of the MPG-CAS student program.

REFERENCES

- Arnaboldi M., et al., 2002, *AJ*, 123, 760
- Barnes J. E., 1992, *ApJ*, 393, 484
- Bell E. F., et al., 2008, *ApJ*, 680, 295
- Belokurov V., et al., 2006, *ApJ*, 642, L137
- Benson A. J., 2005, *MNRAS*, 358, 551
- Binney J., Tremaine S., 2008, *gady.book*,
- Blumenthal G. R., Faber S. M., Primack J. R., Rees M. J., 1984, *Natur*, 311, 517
- Boylan-Kolchin M., Ma C.-P., Quataert E., 2008, *MNRAS*, 383, 93
- Bullock J. S., Johnston K. V., 2005, *ApJ*, 635, 931
- Carollo D., et al., 2010, *ApJ*, 712, 692
- Chandrasekhar S., 1943, *ApJ*, 97, 255
- Cole S., Lacey C. G., Baugh C. M., Frenk C. S., 2000, *MNRAS*, 319, 168
- Cooper A. P., et al., 2010, *MNRAS*, 406, 744
- Cox T. J., Dutta S. N., Di Matteo T., Hernquist L., Hopkins P. F., Robertson B., Springel V., 2006, *ApJ*, 650, 791
- D'Onghia E., Besla G., Cox T. J., Hernquist L., 2009, *Natur*, 460, 605
- Dubinski J., Mihos J. C., Hernquist L., 1996, *ApJ*, 462, 576
- Einasto J., Saar E., Kaasik A., Chernin A. D., 1974, *Natur*, 252, 111
- Faber S. M., Lin D. N. C., 1983, *ApJ*, 266, L17
- Ferguson A. M. N., Johnson R. A., Faria D. C., Irwin M. J., Ibata R. A., Johnston K. V., Lewis G. F., Tanvir N. R., 2005, *ApJ*, 622, L109
- Fontana A., et al., 2004, *A&A*, 424, 23
- Forbes D. A., Beasley M. A., Bekki K., Brodie J. P., Strader J., 2003, *Sci*, 301, 1217
- Gan J., Kang X., van den Bosch F. C., Hou J., 2010, *MNRAS*, 408, 2201
- Gerhard O., Arnaboldi M., Freeman K. C., Kashikawa N., Okamura S., Yasuda N., 2005, *ApJ*, 621, L93
- Gnedin O. Y., 2003, *ApJ*, 582, 141
- Gonzalez A. H., Zabludoff A. I., Zaritsky D., Dalcanton J. J., 2000, *ApJ*, 536, 561
- Hernquist L., 1990, *ApJ*, 356, 359
- Ibata R., Martin N. F., Irwin M., Chapman S., Ferguson A. M. N., Lewis G. F., McConnachie A. W., 2007, *ApJ*, 671, 1591

- Ibata R. A., Gilmore G., Irwin M. J., 1994, *Natur*, 370, 194
- Jiang C. Y., Jing Y. P., Faltenbacher A., Lin W. P., Li C., 2008, *ApJ*, 675, 1095
- Kalirai J. S., Guhathakurta P., Gilbert K. M., Reitzel D. B., Majewski S. R., Rich R. M., Cooper M. C., 2006, *ApJ*, 641, 268
- Kang X., van den Bosch F. C., 2008, *ApJ*, 676, L101
- Kauffmann G., Colberg J. M., Diaferio A., White S. D. M., 1999, *MNRAS*, 307, 529
- Kazantzidis S., Lokas E. L., Callegari S., Mayer L., Moustakas L. A., 2011, *ApJ*, 726, 98
- Kazantzidis S., Mayer L., Mastropietro C., Diemand J., Stadel J., Moore B., 2004, *ApJ*, 608, 663
- Klimontowski J., Lokas E. L., Kazantzidis S., Mayer L., Mamon G. A., 2009, *MNRAS*, 397, 2015
- Klimontowski J., Lokas E. L., Kazantzidis S., Mayer L., Mamon G. A., Prada F., 2009, *MNRAS*, 400, 2162
- Klimontowski J., Lokas E. L., Kazantzidis S., Prada F., Mayer L., Mamon G. A., 2007, *MNRAS*, 378, 353
- Kravtsov A. V., Gnedin O. Y., Klypin A. A., 2004, *ApJ*, 609, 482
- Macciò A. V., Dutton A. A., van den Bosch F. C., 2008, *MNRAS*, 391, 1940
- Macciò A. V., Dutton A. A., van den Bosch F. C., Moore B., Potter D., Stadel J., 2007, *MNRAS*, 378, 55
- Majewski S. R., Skrutskie M. F., Weinberg M. D., Ostriker J. C., 2003, *ApJ*, 599, 1082
- Malin D., Hadley B., 1997, *PASA*, 14, 52
- Martínez-Delgado D., Butler D. J., Rix H.-W., Franco V. I., Peñarrubia J., Alfaro E. J., Dinescu D. I., 2005, *ApJ*, 633, 205
- Martínez-Delgado D., et al., 2012, *ApJ*, 748, L24
- Martin N. F., Ibata R. A., Bellazzini M., Irwin M. J., Lewis G. F., Dehnen W., 2004, *MNRAS*, 348, 12
- Mastropietro C., Moore B., Mayer L., Debattista V. P., Piffaretti R., Stadel J., 2005, *MNRAS*, 364, 607
- Mayer L., Kazantzidis S., Mastropietro C., Wadsley J., 2007, *Natur*, 445, 738
- Mayer L., Governato F., Colpi M., Moore B., Quinn T., Wadsley J., Stadel J., Lake G., 2001, *ApJ*, 559, 754
- Mayer L., Governato F., Colpi M., Moore B., Quinn T., Wadsley J., Stadel J., Lake G., 2001, *ApJ*, 547, L123
- Mayer L., Mastropietro C., Wadsley J., Stadel J., Moore B., 2006, *MNRAS*, 369, 1021
- Mihos J. C., Harding P., Feldmeier J., Morrison H., 2005, *ApJ*, 631, L41
- Monaco P., Murante G., Borgani S., Fontanot F., 2006, *ApJ*, 652, L89
- Moore B., Ghigna S., Governato F., Lake G., Quinn T., Stadel J., Tozzi P., 1999, *ApJ*, 524, L19
- Moster B. P., Somerville R. S., Maubetsch C., van den Bosch F. C., Macciò A. V., Naab T., Oser L., 2010, *ApJ*, 710, 903
- Navarro J. F., Frenk C. S., White S. D. M., 1997, *ApJ*, 490, 493
- Newberg H. J., et al., 2002, *ApJ*, 569, 245
- Peñarrubia J., Navarro J. F., McConnachie A. W., 2008, *ApJ*, 673, 226
- Pohlen M., Martínez-Delgado D., Majewski S., Palma C., Prada F., Balcells M., 2004, *ASPC*, 327, 288
- Somerville R. S., et al., 2008, *ApJ*, 672, 776
- Springel V., 2005, *MNRAS*, 364, 1105
- Springel V., Di Matteo T., Hernquist L., 2005, *MNRAS*, 361, 776
- Taylor J. E., Babul A., 2001, *ApJ*, 559, 716
- Toomre A., Toomre J., 1972, *ApJ*, 178, 623
- Villalobos Á., De Lucia G., Borgani S., Murante G., 2012, *MNRAS*, 424, 2401
- White S. D. M., Rees M. J., 1978, *MNRAS*, 183, 341
- Yanny B., et al., 2000, *ApJ*, 540, 825
- Zentner A. R., Bullock J. S., 2003, *ApJ*, 598, 49
- Zibetti S., White S. D. M., Schneider D. P., Brinkmann J., 2005, *MNRAS*, 358, 949

This paper has been typeset from a \LaTeX file prepared by the author.